NANO LETTERS

pubs.acs.org/NanoLett

Letter

Nanoscale Gap-Plasmon-Enhanced Superconducting Photon Detectors at Single-Photon Level

Jing-Wei Yang, Tzu-Yu Peng, Daniel D. A. Clarke, Frank Daniel Bello, Jia-Wern Chen, Hao-Chen Yeh, Wei-Ren Syong, Chi-Te Liang, Ortwin Hess,* and Yu-Jung Lu*

Cite This: *Nano Lett.* 2023, 23, 11387−11394

Read Online

ACCESS | Metrics & More | Article Recommendations | Supporting Information

ABSTRACT: With a growing demand for detecting light at the single-photon level in various fields, researchers are focused on optimizing the performance of superconducting single-photon detectors (SSPDs) by using multiple approaches. However, input light coupling for visible light has remained a challenge in the development of efficient SSPDs. To overcome these limitations, we developed a novel system that integrates NbN superconducting microwire photon detectors (SMPDs) with gap-plasmon resonators to improve the photon detection efficiency to 98% while preserving all detector performance features, such as polarization insensitivity. The plasmonic SMPDs exhibit a hot-belt effect that generates a nonlinear photoresponse in the visible range operated at 9 K (~0.64T_c), resulting in a 233-fold increase in phonon−electron interaction factor (γ) compared to pristine SMPDs at resonance under CW illumination. These findings open up new opportunities for ultrasensitive single-photon detection in areas like quantum information processing, quantum optics, imaging, and sensing at visible wavelengths.

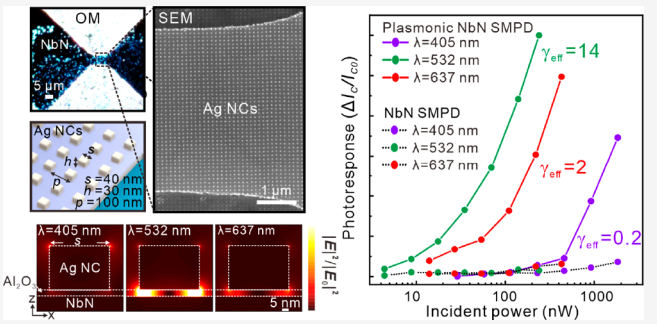

KEYWORDS: *single-photon detection, visible light, gap-plasmon resonance, superconducting photodetectors, NbN, nonlinear photoresponse*

Plasmonic nanostructures can enhance the absorption and detection of photons, leading to improved performance of various types of photodetectors.[1−4] One promising approach is the use of gap-plasmon resonances (GPRs),[5−15] which confine a strong localized electromagnetic field into a small gap between two metallic materials, resulting in strong light−matter interaction, which has various applications in fields such as strong coupling phenomena,[5,6,13] control of the emission such as amplified spontaneous emission and nanolasing nanolasers,[10,11,15] and sensitive photodetectors.[14,16] Detecting light at the single-photon level in quantum photonic systems is crucial; thus, single-photon avalanche detectors (SPADs) and superconducting single-photon detectors (SSPDs) play a significant role in their performance.[26] SSPDs are highly sensitive and have fast response times, making them useful in various applications, including quantum key distribution,[17] optical quantum computing,[18,19] astronomy and dark matter detection,[20,21] satellite laser ranging for LiDAR,[22] and particle physics.[23] The detection efficiency of SSPDs can be improved by using superconducting nanowires with a typical width of 100 nm, which generally have better detection efficiency than microwire-based devices.[24] For optimal detection efficiency and fast response times, the width of the superconducting wire should be comparable to the size of a single photon-induced hot spot, which is around 40 nm for niobium nitride.[25,26] However, sacrifices must be made when adopting these solutions, such as polarization sensitivity,[27] suppression of critical current,[28] and limited absorption coefficient in the visible light range. Thus, superconducting microwires are advantageous due to low kinetic inductance and good fiber coupling efficiency,[29] and plasmonic nanostructures can potentially enhance photon absorption and detection. Using superconducting microwires in large-area photodetectors can simplify the manufacturing process with a high throughput. To improve the photon response in SSPDs, several nanophotonic and plasmonic nanostructure designs have been proposed to increase the detection efficiency of NbN SSPDs,[12,14,16,30,31] including nanomeanders with high filling factors, integration with distributed Bragg reflectors (DBRs), and plasmonic perfect absorbers.[27,32−34] However, these solutions come with trade-offs, such as reduced critical temperature, increased polarization sensitivity, and suppression of the critical current.

Most SSPDs are optimized for high detection efficiency in the near-infrared range.[32,35−41] To date, there have yet to be reports on optimizing SSPDs for visible light due to the

Received: May 8, 2023
Revised: October 26, 2023
Accepted: October 27, 2023
Published: October 31, 2023

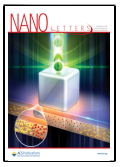

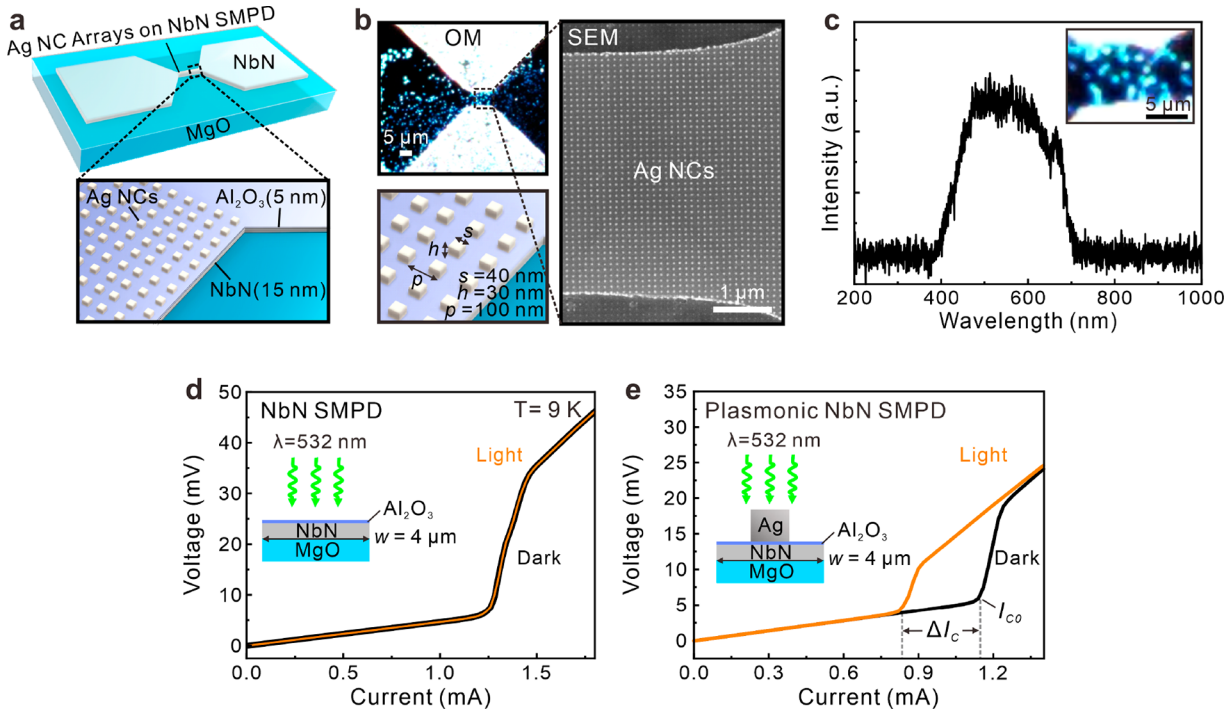

Figure 1. Gap-plasmon-enhanced photodetection in an NbN superconducting microwire photodetector (SMPD). (a) Schematic of the plasmonic SMPD, featuring AgNCs on NbN microwire photodetectors capped with 5 nm Al_2O_3. (b) Dark-field light scattering image and SEM image of the designed plasmonic device. (c) Dark-field scattering spectrum of the gap-plasmon resonance mode from the designed gap-plasmon resonators. (d, e) *IV* curves measured from pristine SMPD and plasmonic SMPD at 9 K, where I_{c0} represents the critical current for the dark state and ΔI_c represents the difference in critical current, serving as a factor indicating the photoresponse.

challenge of input light coupling for visible light remaining an obstacle. To overcome this challenge, we have designed external gap plasmon nanoresonators using particle-on-film nanocavities, resulting in a giant nonlinear photoresponse operated at 9 K via GPR. The key idea in this work is using GPR to enhance the light−matter interaction in the plasmonic photodetectors, resulting in sensitive photon detection at the single-photon level. To control the plasmonic gap for strong light confinement, we capped NbN superconducting microwire single-photon detectors (SMPDs) with a 5 nm thick Al_2O_3 layer by atomic layer deposition and fabricated Ag nanocubes (AgNCs) with a size of 40 nm on top to form gap-plasmon nanoresonators that have plasmon resonance in the visible region. The plasmonic NbN SMPDs achieved a 233-fold enhancement in the photoresponse factor (γ) compared to pristine NbN SMPDs under CW illumination at a resonant wavelength of 532 nm. This giant photoresponse observed in the plasmonic SMPD predominately results from localized heating induced by gap plasmons. We further demonstrated that GPRs that enhance the light−matter interaction can significantly improve the photon detection efficiency of SMPDs to 98% at the single-photon level. Our results show great potential for the development of ultracompact integrated optoelectronic devices with low power consumption and low noise for biomedical imaging, quantum optics, quantum communications, LiDAR, and sensing.

By exploiting the unique properties of GPRs, in combination with superconducting materials, a giant visible-light photoresponse in superconducting phototodetectors can be achieved. To design GPRs based plasmonic nanostructures, our device design contains an ultrathin dielectric layer sandwiched between the NbN microwire and the AgNC as shown in Figure 1a. First, we defined a 15 nm thick NbN wire with a length of 10 μm and a width of 4 μm by photolithography. Subsequently, a 5 nm thick Al_2O_3 layer was used as the dielectric layer on the NbN microwire. Finally, plasmonic AgNC arrays with a period of 100 nm and each AgNC are fabricated 40 nm in length and 30 nm in height on Al_2O_3/NbN (see the Methods section and Figure S1). Figure 1b shows the dark-field optical image and scanning electron microscopy (SEM) images of AgNCs on the NbN microwire capped with 5 nm thick Al_2O_3. Note that the period between two adjacent AgNCs should be at least 100 nm; the calculated results reveal that a confined optical field occurs between the two AgNCs if they are too close. To optimize the plasmonic nanostructures, the GPR mode can be controlled by varying the period of AgNCs and the thickness of the dielectric gap, as shown in Figure S2. The electric field profiles of the GPR modes with varied thickness of Al_2O_3 reveals the 5 nm dielectric gap has the strongest localized EM field (see Figure S3). The material-dependent local electromagnetic field confinement between the metal nanoparticle (Au, Cu, and Ag) and the NbN film was calculated to optimize the device design (see Figure S4). Among the three metals, the particle-on-film nanocavities based on Ag NC result in strong EM field confinement in the gap between the metal particle and the NbN film. As a result, the dark-field scattering spectrum of the optimized plasmonic SMPD (see Figure 1c) indicates the plasmonic resonance wavelength is centered at 500 nm. We used the method of a two-point resistance probe to characterize the GPR-enhanced SMPDs. Figures 1d and 1e show the *IV* curves of the NbN SMPD and plasmonic NbN SMPD in the dark and under illumination at 532 nm with an input power of 70 nW at 9 K, with a fixed width of the NbN

https://doi.org/10.1021/acs.nanolett.3c01703
Nano Lett. 2023, 23, 11387−11394

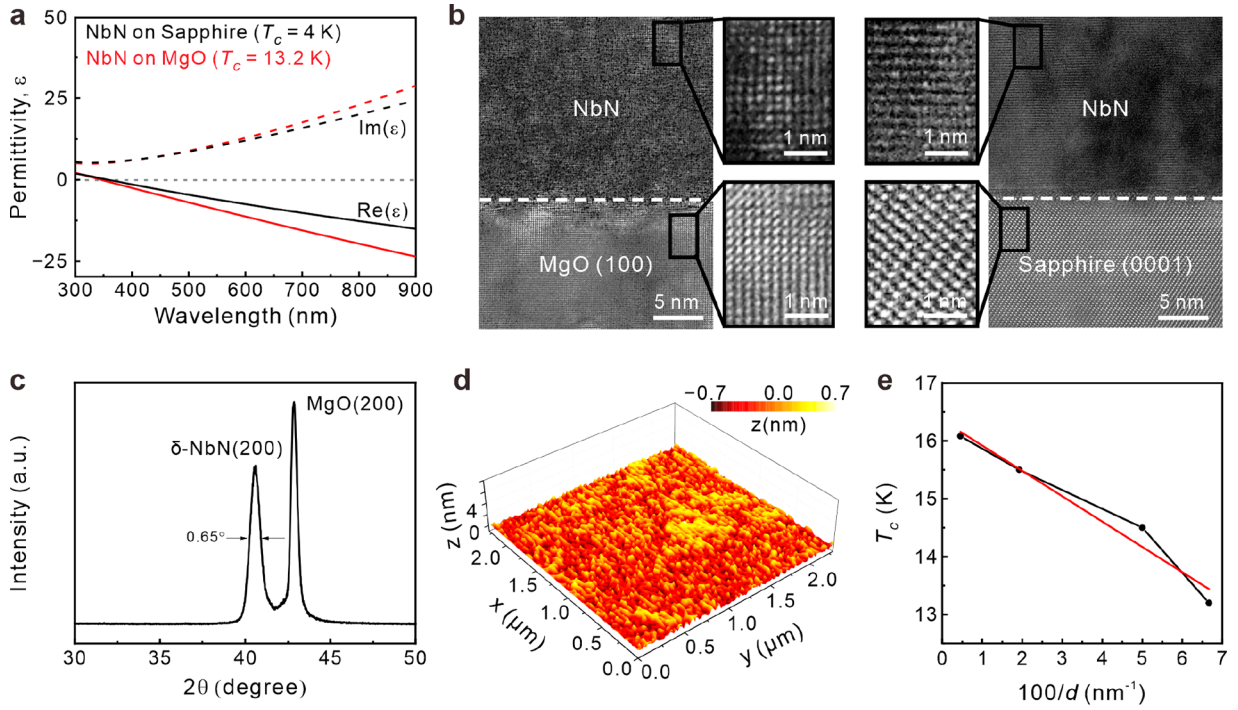

Figure 2. Optimized superconducting properties of quasi-epitaxial NbN films on MgO (100). (a) Dielectric permittivity and critical temperature of NbN films deposited at 800 °C on MgO and c-sapphire substrates. (b) High-resolution cross-sectional transmission electron microscopy (TEM) images show the rock-salt-type lattice structure (δ-NbN) of the NbN film on MgO. (c) X-ray diffraction intensity diagram and (d) atomic force microscopy (AFM) image reveal the atomically smooth surface of the crystalline NbN film on MgO. (e) The critical temperature (T_c) of superconductivity is measured as a function of the film thickness (d), with black points representing T_c measured by SQUID and a red line indicating the fitting model.

nanowire (4 μm). In this work, the photoresponse is defined by the ratio of the difference between the critical currents in the dark and under illumination (ΔI_c) and the critical current in the dark I_{c0}. The critical current is defined as the intersection of the linear extrapolation of the superconducting state and transition state currents, as shown in Figure 1e. We found that the plasmonic NbN SMPD exhibited excellent detection performance, which is directly related to the photoinduced critical current change with a $\Delta I_c/I_{c0}$ of 0.27; however, the NbN SMPD shows no variation in response, whether it is illuminated or not.

As illustrated in Figure 2a, quasi-epitaxial NbN films are grown by radio frequency reactive magnetron sputter on a MgO (100) substrate.[42] We controlled the sputtering parameters with an Ar/N_2 gas flow rate ratio at a substrate temperature of 800 °C to optimize the film quality with both good optically metallic properties and superconductivity. The material properties were characterized by variable angle spectroscopic ellipsometry and a superconducting quantum interference device (SQUID). The complex permittivities ε of NbN films on MgO (100) and sapphire (0001) are described well by the Drude model and Lorentz model (see Tables S1 and S2). Although the NbN films with a fixed thickness of 15 nm on both substrates show optically metallic properties in the visible range, the NbN film on MgO has a more negative real part of permittivity and a higher T_c ($T_c \sim 13.2$ K) than that on the sapphire substrate ($T_c \sim 4$ K). This is due to the lattice constant of MgO (4.21 Å) being closer to that of NbN than that of sapphire (4.78 Å). According to transmission electron microscopy (TEM) images of NbN films on MgO and sapphire (see Figure 2b), the TEM image shows a clear cubic structure with a lattice constant of 4.44 Å in the quasi-epitaxial NbN film on MgO. In addition, the X-ray diffraction pattern, as shown in Figure 2c, discloses the feature of δ-NbN on MgO, which usually has higher T_c among all types of NbN (see Figures S5 and S6).[43] The surface morphology is obtained by atomic force microscopy (AFM), as shown in Figure 2d, and it exhibits an ultralow root-mean-square (RMS) roughness of 2.5 Å. This roughness plays a key role in the subsequent nanofabrication of NbN nanowires because we plan to fabricate many nanostructures on large and flat films. Figure 2e shows the T_c values with various NbN thicknesses on MgO. We fitted T_c as a function of the inverse of thickness, d, by the Simonin model: $T_c = T_{c,bluk}(1 - d_c/d)$, and we find that the critical temperature of the bulk $T_{c,bluk}$ is 16.4 K and that the critical thickness d_c is 2.7 nm.[44] The suppression of T_c as the thickness decreases can be attributed to the defects and granularity in thinner NbN films.[45]

In addition, the plasmonic NbN SMPD reveals strong wavelength-dependent photodetection, as shown in Figures 3a and S7. We used continuous-wave (CW) lasers with focused spot sizes of 1 μm at wavelengths of 405, 532, and 637 nm as visible light sources; these lasers are normally incident on the microwire and are focused through a 100× objective lens. The imperfection of the nanofabrication process would result in a slight difference in critical current (I_{c0}) between plasmonic NbN SMPD and pristine NbN SMPD without illumination. Thus, we use a photoinduced critical current change ($\Delta I_c/I_{c0}$), which directly relates to the detection performance for discussing the effect of adding plasmonic nanoparticles. GPR-enhanced photodetection can be observed at all visible wavelengths, which leads to a drastic photoresponse $\Delta I_c/I_{c0}$ at 532 nm with the lowest detectable power of 4.4 nW. When the power is approximately 220 nW, the plasmonic NbN SMPD

https://doi.org/10.1021/acs.nanolett.3c01703
Nano Lett. 2023, 23, 11387−11394

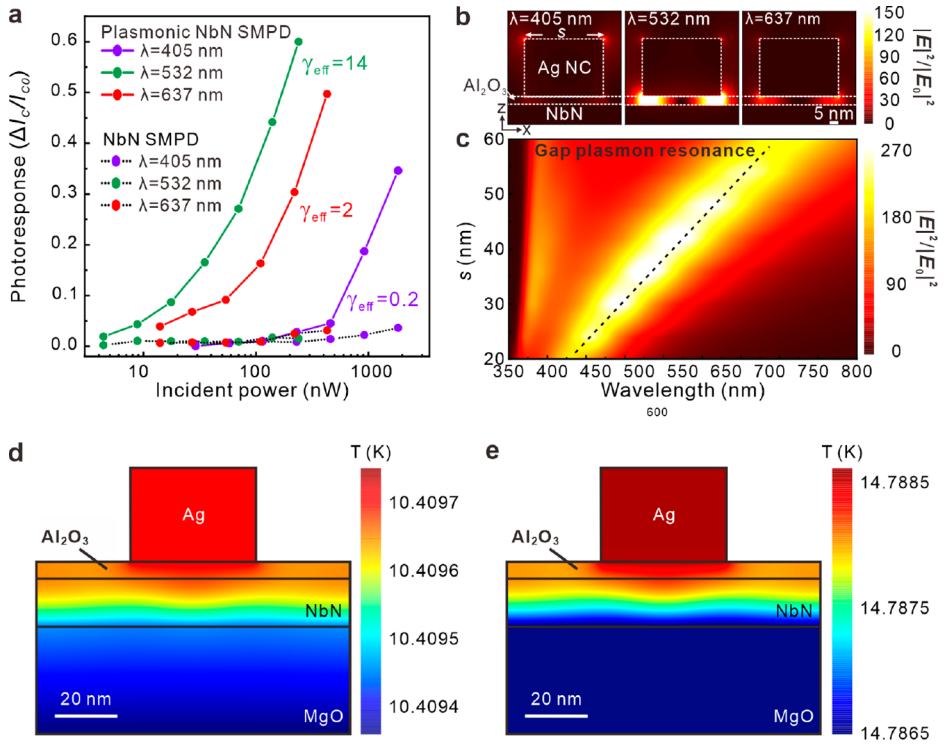

Figure 3. Working principle of giant nonlinear photoresponse in superconducting microwire photodetector (SMPD) with gap-plasmon resonators. (a) The photoinduced change in critical current as a function of incident power with different wavelengths (405, 532, and 637 nm) is measured at 9 K, revealing a significant nonlinear photoresponse in NbN SMPD with gap-plasmon resonances (solid line). The dashed line represents the photoresponse from pristine NbN SMPD. (b) Simulated electric-field enhancement for the plasmonic nanostructures at a different wavelengths, demonstrating the wavelength-dependent plasmonic coupling between the Ag NC and the NbN film. (c) Color map of numerically calculated $|E|^2/|E_0|^2$ spectra as a function of the size of the AgNC with a fixed periodicity of 100 nm. The peak of the gap plasmon resonances undergoes a spectral red-shift with increasing the size of AgNC. (d) Steady-state temperature distribution for a two-dimensional cross section of the plasmonic SMPD under an illumination intensity of 220 nW/μm^2. (e) The NbN wire is heated beyond its critical temperature (approximately 13.2 K) under an illumination intensity of 1800 nW/μm^2.

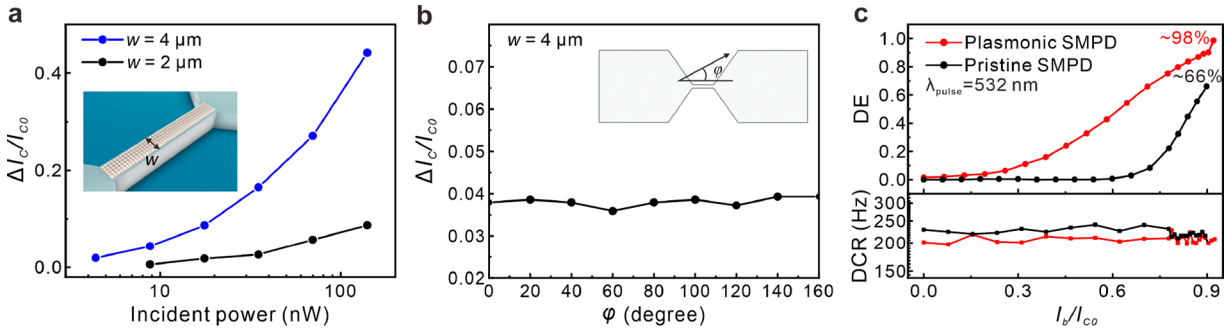

Figure 4. Device performance of NbN SMPDs with gap-plasmon resonators. (a) The change in critical current induced by incident power was measured at 9 K for different photodetectors with varying widths of NbN microwire, using incident light with a wavelength of 532 nm. (b) The angle-dependent change in critical current measured at 9 K revealed polarization-independent photodetection signatures, where φ represents the angle between the nanowire and polarized light with a wavelength of 637 nm. (c) Normalized bias-current dependence of photon detection efficiency (DE) of plasmonic SMPD, pristine SMPD, and their dark count rate (DCR). The plasmonic SMPD demonstrated exceptional performance, achieving 98% detection efficiency when detecting visible photons at a single-photon level.

has maximal $\Delta I_c/I_{c0}$ values of 0.6 at 532 nm, 0.3 at 637 nm, and 0.03 at 405 nm. These results of the photoresponse are consistent with the dark field scattering spectrum in Figure 1c. The gap-plasmon-enhanced photoresponse of ΔI_c can be fitted by Vodolazov's hot-belt model[46,47] (see Figure S8), which assumes that heated electrons have been thermalized with phonons when they reach the edges of the wire and form a hot belt with a size of approximately $w \times w$. A factor of γ, which is proportional to the ratio of the specific heat capacities of the electron and phonon, is used to describe the portion of the photon's energy that is transferred to electrons. The gap plasmon mode can enhance the thermalization of heated electrons and lead to a larger effective γ, γ_{eff}. We found that the wavelength-dependent γ_{eff} at 405, 532, and 637 nm are 0.2, 14, and 2, respectively, which are significantly larger than γ_{eff} of NbN SMPD (γ_{eff} are 0.018, 0.06, and 0.08 at 405, 532, and 637 nm, respectively).

https://doi.org/10.1021/acs.nanolett.3c01703
Nano Lett. 2023, 23, 11387−11394

To elucidate the mechanism by which GPR facilitates enhanced photoresponse, we perform numerical simulations that characterize the electrodynamic and electrothermal responses of the heterostructure under CW illumination (see Note S2). Figure 3b presents the distribution of the electric field enhancement in a cross section of the device, obtained by means of finite-difference time-domain calculations. We observe that the plasmonic NbN film and AgNC support GPR at 532 nm, signified by a strongly localized electromagnetic field in the Al_2O_3 layer that enhances the local absorption of visible photons. In contrast, illumination at 405 and 637 nm is well detuned from the GPR, leading to relatively weak localized fields. Figure 3c shows that the calculated GPR spectra vary with the side width of the AgNCs. The position of the resonance red-shifts when s increases and covers the whole visible region. Crucially, the electric field enhancement is concentrated in only a small spatial region of the device compared to the larger portion of the structure whose steady-state temperature is determined by the cryogenic head and input laser power. Indeed, according to our finite-element heating simulations that explicitly incorporate EM power dissipation in the device (see Note S8), the plasmon-induced heating under 532 nm illumination leads to steady-state temperature increments on the order of a millikelvin or less, as shown in Figure 3d for an intensity of 220 nW/μm^2. Invoking the hot-belt model once more,[46,47] assuming a critical temperature of 13.2 K, consistent with the NbN wire thickness (see Figure 2e), and considering input powers over an equal area of 220 and 70 nW, we predict changes to the critical current of approximately 40% and 28%, respectively, in reasonable agreement with the reported experimental data. Furthermore, it is notable that under a substantially higher intensity of 1800 nW/μm^2, our simulations indicate that the NbN wire is heated beyond its critical temperature (see Figure 3e), suggesting a local breakdown of the superconducting state entirely and thereby the emergence of a conventionally resistive region.

Figure 4a compares two plasmonic NbN SMPDs with different widths of 2 and 4 μm, respectively. It is worth noting that the wider plasmonic NbN SMPD has relatively high sensitivity, which is quite different from the case of standard SMPDs. This is because illuminating the wider plasmonic NbN SMPD can excite more gap-plasmon resonators. Even though the focused spot has a diameter of 1 μm, which is smaller than the width of both detectors, nearly all the photons (99.99%) are spread out within an area of 3 μm in diameter. This means that the plasmonic NbN SMPD, which is only 2 μm wide, might not be able to catch all the photons because they are scattered over a wider area. Therefore, some photons may not be detected by the 2 μm wide detector. Additionally, the wide plasmonic SMPD has other advantages. Numerous reports indicate that reducing the size of the device leads to the suppression of superconductivity.[27,45,48] However, T_c can be maintained in a microwire with the same value in bulk. On the other hand, the wider plasmonic SMPD implies that the device has a higher critical current, which can increase the signal-to-noise ratio. Finally, the kinetic inductance, $L_k \sim l/(wd)$, of the device itself determines its rising time, $\tau_{rise} = L_k/(R_{shunt} + R_N)$, and falling time, $\tau_{fall} = L_k/R_{shunt}$, where l is the total length of the wire.[29,49−51] Therefore, fabricating the SMPD with a reasonable detection area with a broader and shorter microwire can result in a fast switching time. Figure 4b shows that the photodetection of the GPR-enhanced SMPD is independent of the angle φ between the polarization of light and the direction of the microwire, where the incident light has a wavelength of 637 nm and a power of 116 μW with the cryogenic temperature set at 9 K. Because the width of the microwire is larger than the wavelength of visible light and AgNCs are symmetric in geometry, there is no difference in the $I-V$ curve for any polarization.

Compared to the nanowire meander structure of SNSPDs, the absorption characteristics of SNSPDs determine that the intrinsic sensitivity depends on the polarization states of incident light,[27] which can lead to restrictions in certain applications. For example, the information on the QKD depends on the phase difference between two nearby photons and is not related to the polarization of photons. However, the polarization state may fluctuate during the process of fiber-optic transmissions, which results in an unpredictable bit-error rate in the readout of an SNSPD.[52,53] This fact shows the potential for our plasmonic NbN SMPD to detect photons, because the quantum efficiency remains the same regardless of which polarization of light is used for illumination.

To determine the photon-detection efficiency of single visible photons, a pulsed laser with a wavelength of 532 nm, a pulse width of 100 ps, and a repetition rate of 2.5 MHz was used, and the input power was attenuated to the few-photon level (see Note S9). Figure 4c shows the measured photon detection efficiency (DE) and dark count rate (DCR) versus the normalized bias current I_b/I_{c0} for both plasmonic SMPD and pristine SMPD. Note that the optical response we observed is not related to the DCR. It is worth mentioning that the pristine SMPD exhibits a measured detection efficiency of 66%. This is due to the fact that individual visible photons possess sufficient energy to disrupt Cooper pairs within a superconductor, consequently leading to the breakdown of the superconducting state. Thus, by integrating gap plasmon nanostructures to enhance the detection capabilities of the detectors, an impressive detection efficiency of 98% for visible photons in the plasmonic SMPD can be achieved. This optimized detection efficiency can be attributed to the strong electromagnetic field confinement within the gap Al_2O_3 layer that enhances the light−matter interaction. Hence, an investigation of nonequilibrium dynamics is forthcoming, given the apparent breakdown of the superconducting state under a low-powered pulsed laser with a pulse width of 100 ps.

In conclusion, our results demonstrate a significant improvement in the performance of plasmonic NbN SMPDs by using GPRs to enhance the light−matter interaction in the visible. The particle-on-film nanocavities created by arrays of AgNCs on an atomically smooth NbN microstrip capped with 5 nm thick Al_2O_3 have resulted in a giant photoresponse enhancement of 233 compared to pristine NbN SMPDs under CW illumination. The enhancement factor of photoresponse is defined by γ, which is an order of magnitude higher than recently reported SSPDs through diverse structural optimizations (see Table S4).[32,35−38] This enhancement predominately results from the localized heating induced by gap plasmons, causing a transition from the superconducting state to the normal state. In addition, the designed plasmonic NbN SMPDs have multiple advantages, including polarization independence, low kinetic inductance, large active area, and high photoresponse in the visible spectrum. Furthermore, it is worth noting that the plasmonic SMPD can achieve an impressive detection efficiency of 98% for visible photons at a single-photon level under pulsed laser illumination. Because

https://doi.org/10.1021/acs.nanolett.3c01703
Nano Lett. 2023, 23, 11387−11394

the time scale of the plasmon−photon interaction is much shorter than the thermalization, the optimized detection efficiency can be attributed to the gap plasmon mode that enhances the light−matter interaction, leading to the efficient disruption of Cooper pairs and the consequent breakdown of the superconducting state. Therefore, we expect these plasmonic SMPDs to have a lower dark count rate, lower time jitter, and higher single-photon detection efficiency for visible-light detection, making them promising candidates for various applications.

METHODS

Device Fabrication. The complete fabrication process is described in the Supporting Information. The structure of the NbN microwire is defined by a direct writer (Heidelberg, iNSTRUMENTS); then, 30 nm thick chromium is used as a hard mask and dry etched by CF_4. Then, 5 nm thick Al_2O_3 is deposited by atomic layer deposition (ALD, a custom-designed system produced by the local company Syskey Technology). Finally, we utilize electron-beam lithography (ELS-7000 (ELIONIX)) combined with electron-beam evaporation (ULVAC E-beam Evaporator, Peva-400E) to fabricate a 40 nm long and 30 nm high AgNC array on Al_2O_3.

Characterization of the Photodetector at Cryogenic Temperatures. The measured resistance of the metallic NbN microwire (R_N) is 250 Ω at room temperature. At 9 K, a Keithley 2400 was used as a current source to provide a sweeping current that flows through the NbN microwire and a shunt resistor (R_{shunt}) of 32 Ω, and we measured the voltage difference between the two ends using the Keithley 2400. The device was measured by using a confocal laser scanning microscope system equipped with a vibration-free, closed-cycle cryostat (Attodry 800, Attocube).

ASSOCIATED CONTENT

Supporting Information

The Supporting Information is available free of charge at https://pubs.acs.org/doi/10.1021/acs.nanolett.3c01703.

Additional experimental details of the preparation and characterization of quasi-epitaxial NbN films; device fabrication; plasmonic nanostructure design; SQUID measurements; wavelength-dependent photoresponse; performance metrics of superconducting photon detectors; simulation of electromagnetic heating (PDF)

AUTHOR INFORMATION

Corresponding Authors

Yu-Jung Lu − *Research Center for Applied Sciences, Academia Sinica, Taipei 11529, Taiwan; Graduate Institute of Applied Physics, National Taiwan University, Taipei 10617, Taiwan;* orcid.org/0000-0002-3932-653X; Email: yujunglu@gate.sinica.edu.tw

Ortwin Hess − *School of Physics and CRANN Institute, Trinity College Dublin, Dublin 2 D02 PN40, Ireland; Blackett Laboratory, Imperial College London, South Kensington Campus, SW7 2AZ London, United Kingdom;* orcid.org/0000-0002-6024-0677; Email: Ortwin.Hess@tcd.ie

Authors

Jing-Wei Yang − *Research Center for Applied Sciences, Academia Sinica, Taipei 11529, Taiwan; Graduate Institute of Applied Physics, National Taiwan University, Taipei 10617, Taiwan*

Tzu-Yu Peng − *Research Center for Applied Sciences, Academia Sinica, Taipei 11529, Taiwan; Graduate Institute of Applied Physics, National Taiwan University, Taipei 10617, Taiwan*

Daniel D. A. Clarke − *School of Physics and CRANN Institute, Trinity College Dublin, Dublin 2 D02 PN40, Ireland*

Frank Daniel Bello − *School of Physics and CRANN Institute, Trinity College Dublin, Dublin 2 D02 PN40, Ireland*

Jia-Wern Chen − *Research Center for Applied Sciences, Academia Sinica, Taipei 11529, Taiwan*

Hao-Chen Yeh − *Department of Physics, National Taiwan University, Taipei 10617, Taiwan*

Wei-Ren Syong − *Research Center for Applied Sciences, Academia Sinica, Taipei 11529, Taiwan*

Chi-Te Liang − *Graduate Institute of Applied Physics and Department of Physics, National Taiwan University, Taipei 10617, Taiwan*

Complete contact information is available at: https://pubs.acs.org/10.1021/acs.nanolett.3c01703

Author Contributions

Y.J.L. led the project, proposed the idea, and designed all experimental investigations, simulations of localized electromagnetic field distributions, and data analysis. J.W.Y. designed and fabricated devices, performed all the experiments and FDTD calculations, and conducted device characterization. T.Y.P. performed the ellipsometry measurement and helped with the growth of the NbN film. D.D.A.C., F.D.B., and O.H. contributed to the theoretical explanations. H.C.Y. and C.T.L. performed the SQUID measurement to analyze the critical temperature of superconductivity. W.R.S. and J.W.C. helped with the device fabrications. J.W.Y. and Y.J.L. wrote the first version of the manuscript. Y.J.L., D.D.A.C., F.D.B., and O.H. revised the manuscript, and all authors discussed the results and commented on the manuscript.

Notes

The authors declare no competing financial interest.

ACKNOWLEDGMENTS

The authors thank Prof. Harald Giessen at the University of Stuttgart for useful discussions. We thank Li-Chien Chang and Xing-Hao Lee for assisting with device fabrication. We also acknowledge the use of spectroscopic ellipsometry supported by Prof. Yia-Chung Chang. We are grateful to Feng-Yang Tsai, Hsin-Yeh Wu, and Prof. Stathes Paganis for assisting in setting and measuring photon detection efficiency. We acknowledge financial support from the National Science and Technology Council, Taiwan (Grants NSTC-109-2112-M-001-043-MY3 and NSTC-110-2124-M-001-008-MY3), Academia Sinica of Taiwan (AS-CDA-108-M08, AS-GC-110-02), and the Science Foundation of Ireland (SFI) Grant 18/RP/6236.

REFERENCES

(1) Knight, M. W.; Sobhani, H.; Nordlander, P.; Halas, N. J. Photodetection with active optical antennas. *Science* **2011**, *332* (6030), 702−704.

(2) Mühlschlegel, P.; Eisler, H.-J.; Martin, O. J. F.; Hecht, B.; Pohl, D. W. Resonant optical antennas. *Science* **2005**, *308* (5728), 1607−1609.

(3) Schuller, J. A.; Barnard, E. S.; Cai, W.; Jun, Y. C.; White, J. S.; Brongersma, M. L. Plasmonics for extreme light concentration and manipulation. *Nat. Mater.* **2010**, *9* (3), 193−204.
(4) Atwater, H. A.; Polman, A. Plasmonics for improved photovoltaic devices. *Nat. Mater.* **2010**, *9* (3), 205−213.
(5) Chikkaraddy, R.; de Nijs, B.; Benz, F.; Barrow, S. J.; Scherman, O. A.; Rosta, E.; Demetriadou, A.; Fox, P.; Hess, O.; Baumberg, J. J. Single-molecule strong coupling at room temperature in plasmonic nanocavities. *Nature* **2016**, *535* (7610), 127−130.
(6) Leng, H.; Szychowski, B.; Daniel, M.-C.; Pelton, M. Strong coupling and induced transparency at room temperature with single quantum dots and gap plasmons. *Nat. Commun.* **2018**, *9* (1), 4012.
(7) Wang, D.; Koh, Y. R.; Kudyshev, Z. A.; Maize, K.; Kildishev, A. V.; Boltasseva, A.; Shalaev, V. M.; Shakouri, A. Spatial and temporal nanoscale plasmonic heating quantified by thermoreflectance. *Nano Lett.* **2019**, *19* (6), 3796−3803.
(8) Lassiter, J. B.; McGuire, F.; Mock, J. J.; Ciracì, C.; Hill, R. T.; Wiley, B. J.; Chilkoti, A.; Smith, D. R. Plasmonic waveguide modes of film-coupled metallic nanocubes. *Nano Lett.* **2013**, *13* (12), 5866−5872.
(9) Stewart, J. W.; Nebabu, T.; Mikkelsen, M. H. Control of nanoscale heat generation with lithography-free metasurface absorbers. *Nano Lett.* **2022**, *22* (13), 5151−5157.
(10) Akselrod, G. M.; Argyropoulos, C.; Hoang, T. B.; Ciracì, C.; Fang, C.; Huang, J.; Smith, D. R.; Mikkelsen, M. H. Probing the mechanisms of large Purcell enhancement in plasmonic nanoantennas. *Nat. Commun.* **2014**, *8* (11), 835−840.
(11) Hsieh, Y.-H.; Hsu, B.-W.; Peng, K.-N.; Lee, K.-W.; Chu, C. W.; Chang, S.-W.; Lin, H.-W.; Yen, T.-J.; Lu, Y.-J. Perovskite quantum dot lasing in a gap-plasmon nanocavity with ultralow threshold. *ACS Nano* **2020**, *14* (9), 11670−11676.
(12) Tong, J.; Suo, F.; Ma, J.; Tobing, L. Y. M.; Qian, L.; Zhang, D. H. Surface plasmon enhanced infrared photodetection. *Opto-Electronic Advances* **2019**, *2* (1), 1800261−10.
(13) Scholl, J. A.; García-Etxarri, A.; Koh, A. L.; Dionne, J. A. Observation of quantum tunneling between two plasmonic nanoparticles. *Nano Lett.* **2013**, *13* (2), 564−569.
(14) Wu, Z.-Q.; Yang, J.-L.; Manjunath, N. K.; Zhang, Y.-J.; Feng, S.-R.; Lu, Y.-H.; Wu, J.-H.; Zhao, W.-W.; Qiu, C.-Y.; Li, J.-F.; Lin, S.-S. Gap-mode surface-plasmon-enhanced photoluminescence and photoresponse of MoS2. *Adv. Mater.* **2018**, *30* (27), 1706527.
(15) Lumdee, C.; Yun, B.; Kik, P. G. Gap-plasmon enhanced gold nanoparticle photoluminescence. *ACS Photonics* **2014**, *1* (11), 1224−1230.
(16) Sun, B.; Wang, Z.; Liu, Z.; Tan, X.; Liu, X.; Shi, T.; Zhou, J.; Liao, G. Tailoring of silver nanocubes with optimized localized surface plasmon in a gap mode for a flexible MoS_2 photodetector. *Adv. Funct. Mater.* **2019**, *29* (26), 1900541.
(17) Takesue, H.; Nam, S. W.; Zhang, Q.; Hadfield, R. H.; Honjo, T.; Tamaki, K.; Yamamoto, Y. Quantum key distribution over a 40-dB channel loss using superconducting single-photon detectors. *Nat. Commun.* **2007**, *1* (6), 343−348.
(18) Zhong, H.-S.; Wang, H.; Deng, Y.-H.; Chen, M.-C.; Peng, L.-C.; Luo, Y.-H.; Qin, J.; Wu, D.; Ding, X.; Hu, Y.; Hu, P.; Yang, X.-Y.; Zhang, W.-J.; Li, H.; Li, Y.; Jiang, X.; Gan, L.; Yang, G.; You, L.; Wang, Z.; Li, L.; Liu, N.-L.; Lu, C.-Y.; Pan, J.-W. Quantum computational advantage using photons. *Science* **2020**, *370* (6523), 1460−1463.
(19) Varnava, M.; Browne, D. E.; Rudolph, T. How good must single photon sources and detectors be for efficient linear optical quantum computation? *Phys. Rev. Lett.* **2008**, *100* (6), 060502.
(20) Wollman, E. E.; Verma, V. B.; Walter, A. B.; Chiles, J.; Korzh, B.; Allmaras, J. P.; Zhai, Y.; Lita, A. E.; McCaughan, A. N.; Schmidt, E.; Frasca, S.; Mirin, R. P.; Nam, S. W.; Shaw, M. D. Recent advances in superconducting nanowire single-photon detector technology for exoplanet transit spectroscopy in the mid-infrared. *Journal of Astronomical Telescopes, Instruments, and Systems* **2021**, *7* (1), 1−10.
(21) Hochberg, Y.; Charaev, I.; Nam, S.-W.; Verma, V.; Colangelo, M.; Berggren, K. K. Detecting sub-GeV dark matter with superconducting nanowires. *Phys. Rev. Lett.* **2019**, *123* (15), 151802.
(22) Taylor, G. G.; Morozov, D.; Gemmell, N. R.; Erotokritou, K.; Miki, S.; Terai, H.; Hadfield, R. H. Photon counting LIDAR at 2.3μm wavelength with superconducting nanowires. *Opt. Express* **2019**, *27* (26), 38147−38158.
(23) Križan, P.; Korpar, S. Photodetectors in particle physics experiments. *Annual Review of Nuclear and Particle Science* **2013**, *63* (1), 329−349.
(24) Korneeva, Y. P.; Vodolazov, D. Y.; Semenov, A. V.; Florya, I. N.; Simonov, N.; Baeva, E.; Korneev, A. A.; Goltsman, G. N.; Klapwijk, T. M. Optical single-photon detection in micrometer-scale NbN bridges. *Phys. Rev. Appl.* **2018**, *9* (6), 064037.
(25) Wördenweber, R.; Moshchalkov, V.; Bending, S.; Tafuri, F. *Superconductors at the Nanoscale: From Basic Research to Applications*; De Gruyter: Berlin, 2017.
(26) Hadfield, R. H. Single-photon detectors for optical quantum information applications. *Nat. Commun.* **2009**, *3* (12), 696−705.
(27) Semenov, A.; Günther, B.; Böttger, U.; Hübers, H. W.; Bartolf, H.; Engel, A.; Schilling, A.; Ilin, K.; Siegel, M.; Schneider, R.; Gerthsen, D.; Gippius, N. A. Optical and transport properties of ultrathin NbN films and nanostructures. *Phys. Rev. B* **2009**, *80* (5), 054510.
(28) Zhang, L.; You, L.; Yang, X.; Wu, J.; Lv, C.; Guo, Q.; Zhang, W.; Li, H.; Peng, W.; Wang, Z.; Xie, X. Hotspot relaxation time of NbN superconducting nanowire single-photon detectors on various substrates. *Sci. Rep.* **2018**, *8* (1), 1486.
(29) Zotova, A. N.; Vodolazov, D. Y. Photon detection by current-carrying superconducting film: a time-dependent Ginzburg-Landau approach. *Phys. Rev. B* **2012**, *85* (2), 024509.
(30) Lan, H.-Y.; Hsieh, Y.-H.; Chiao, Z.-Y.; Jariwala, D.; Shih, M.-H.; Yen, T.-J.; Hess, O.; Lu, Y.-J. Gate-tunable plasmon-enhanced photodetection in a monolayer MoS_2 phototransistor with ultrahigh photoresponsivity. *Nano Lett.* **2021**, *21* (7), 3083−3091.
(31) Ni, Z.; Ma, L.; Du, S.; Xu, Y.; Yuan, M.; Fang, H.; Wang, Z.; Xu, M.; Li, D.; Yang, J.; Hu, W.; Pi, X.; Yang, D. Plasmonic silicon quantum dots enabled high-sensitivity ultrabroadband photodetection of graphene-based hybrid phototransistors. *ACS Nano* **2017**, *11* (10), 9854−9862.
(32) Zhang, W.; You, L.; Li, H.; Huang, J.; Lv, C.; Zhang, L.; Liu, X.; Wu, J.; Wang, Z.; Xie, X. NbN superconducting nanowire single photon detector with efficiency over 90% at 1550 nm wavelength operational at compact cryocooler temperature. *Science China Physics, Mechanics & Astronomy* **2017**, *60* (12), 120314.
(33) Akhlaghi, M. K.; Schelew, E.; Young, J. F. Waveguide integrated superconducting single-photon detectors implemented as near-perfect absorbers of coherent radiation. *Nat. Commun.* **2015**, *6* (1), 8233.
(34) Wang, H.; Qin, J.; Ding, X.; Chen, M.-C.; Chen, S.; You, X.; He, Y.-M.; Jiang, X.; You, L.; Wang, Z.; Schneider, C.; Renema, J. J.; Höfling, S.; Lu, C.-Y.; Pan, J.-W. Boson sampling with 20 input photons and a 60-mode interferometer in a 10̂14-dimensional hilbert space. *Phys. Rev. Lett.* **2019**, *123* (25), 250503.
(35) Hakimi, I.; Vardi, N.; Sharoni, A.; Rosenbluh, M.; Yeshurun, Y. Enhancement of photon detection in superconducting nanowire single photon detector exposed to oscillating magnetic field. *Appl. Phys. Lett.* **2021**, *118* (23), 232603.
(36) Zhang, W.; Jia, Q.; You, L.; Ou, X.; Huang, H.; Zhang, L.; Li, H.; Wang, Z.; Xie, X. Saturating intrinsic detection efficiency of superconducting nanowire single-photon detectors *via* defect engineering. *Phys. Rev. Appl.* **2019**, *12* (4), 044040.
(37) Heath, R. M.; Tanner, M. G.; Drysdale, T. D.; Miki, S.; Giannini, V.; Maier, S. A.; Hadfield, R. H. Nanoantenna enhancement for telecom-wavelength superconducting single photon detectors. *Nano Lett.* **2015**, *15* (2), 819−822.
(38) Lv, C.; Zhang, W.; You, L.; Hu, P.; Wang, H.; Li, H.; Zhang, C.; Huang, J.; Wang, Y.; Yang, X.; Wang, Z.; Xie, X. Improving maximum count rate of superconducting nanowire single-photon detector with

https://doi.org/10.1021/acs.nanolett.3c01703
Nano Lett. 2023, 23, 11387−11394

small active area using series attenuator. *AIP Adv.* **2018**, *8* (10), 105018.
(39) Csete, M.; Szekeres, G.; Szenes, A.; Szalai, A.; Szabó, G. Plasmonic structure integrated single-photon detector configurations to improve absorptance and polarization contrast. *Sensors* **2015**, *15* (2), 3513−3539.
(40) Verma, V. B.; Marsili, F.; Harrington, S.; Lita, A. E.; Mirin, R. P.; Nam, S. W. A three-dimensional, polarization-insensitive superconducting nanowire avalanche photodetector. *Appl. Phys. Lett.* **2012**, *101* (25), 251114.
(41) Tóth, B.; Szenes, A.; Maráczi, D.; Bánhelyi, B.; Csendes, T.; Csete, M. Polarization independent high absorption efficiency single-photon detectors based on three-dimensional integrated superconducting and plasmonic patterns. *IEEE J. Sel. Top. Quantum Electron.* **2020**, *26* (3), 1−9.
(42) Karl, P.; Mennle, S.; Ubl, M.; Flad, P.; Yang, J.-W.; Peng, T.-Y.; Lu, Y.-J.; Giessen, H. Niobium nitride plasmonic perfect absorbers for tunable infrared superconducting nanowire photodetection. *Opt. Express* **2021**, *29* (11), 17087−17096.
(43) Martienssen, W.; Warlimont, H. *Springer Handbook of Condensed Matter and Materials Data*; Springer: Berlin, 2005.
(44) Simonin, J. Surface term in the superconductive Ginzburg-Landau free energy: application to thin films. *Phys. Rev. B* **1986**, *33* (11), 7830−7832.
(45) Ivry, Y.; Kim, C.-S.; Dane, A. E.; De Fazio, D.; McCaughan, A. N.; Sunter, K. A.; Zhao, Q.; Berggren, K. K. Universal scaling of the critical temperature for thin films near the superconducting-to-insulating transition. *Phys. Rev. B* **2014**, *90* (21), 214515.
(46) Vodolazov, D. Y. Single-photon detection by a dirty current-carrying superconducting strip based on the kinetic-equation approach. *Phys. Rev. Appl.* **2017**, *7* (3), 034014.
(47) Bulaevskii, L. N.; Graf, M. J.; Kogan, V. G. Vortex-assisted photon counts and their magnetic field dependence in single-photon superconducting detectors. *Phys. Rev. B* **2012**, *85* (1), 014505.
(48) Martins, B. P. *New Frontiers in superconductivity research*; NOVA Publishers: New York, 2006.
(49) Kerman, A. J.; Dauler, E. A.; Keicher, W. E.; Yang, J. K. W.; Berggren, K. K.; Gol'tsman, G.; Voronov, B. Kinetic-inductance-limited reset time of superconducting nanowire photon counters. *Appl. Phys. Lett.* **2006**, *88* (11), 111116.
(50) Vetter, A.; Ferrari, S.; Rath, P.; Alaee, R.; Kahl, O.; Kovalyuk, V.; Diewald, S.; Goltsman, G. N.; Korneev, A.; Rockstuhl, C.; Pernice, W. H. P. Cavity-enhanced and ultrafast superconducting single-photon detectors. *Nano Lett.* **2016**, *16* (11), 7085−7092.
(51) Marsili, F.; Najafi, F.; Dauler, E.; Bellei, F.; Hu, X.; Csete, M.; Molnar, R. J.; Berggren, K. K. Single-photon detectors based on ultranarrow superconducting nanowires. *Nano Lett.* **2011**, *11* (5), 2048−2053.
(52) Gleim, A. V.; Egorov, V. I.; Nazarov, Y. V.; Smirnov, S. V.; Chistyakov, V. V.; Bannik, O. I.; Anisimov, A. A.; Kynev, S. M.; Ivanova, A. E.; Collins, R. J.; Kozlov, S. A.; Buller, G. S. Secure polarization-independent subcarrier quantum key distribution in optical fiber channel using BB84 protocol with a strong reference. *Opt. Express* **2016**, *24* (3), 2619−2633.
(53) Meng, Y.; Zou, K.; Hu, N.; Xu, L.; Lan, X.; Steinhauer, S.; Gyger, S.; Zwiller, V.; Hu, X. Fractal superconducting nanowires detect infrared single photons with 84% system detection efficiency, 1.02 polarization sensitivity, and 20.8 ps timing resolution. *ACS Photonics* **2022**, *9* (5), 1547−1553.

https://doi.org/10.1021/acs.nanolett.3c01703
Nano Lett. 2023, 23, 11387−11394